Nonlinear implementation of Finite Fracture Mechanics: A case study on notched Brazilian disk samples

International Journal of Non-Linear Mechanics manuscript No.
(will be inserted by the editor)

Nonlinear implementation of Finite Fracture Mechanics: A case study on notched Brazilian disk samples.

Aurélien Doitrand[1], **Alberto Sapora**[2]

[1] Université Grenoble-Alpes - CNRS UMR 5266, SIMaP, F-38000 Grenoble, France
[2] Department of Structural, Geotechnical and Building Engineering, Politecnico di Torino, Turin, Italy

Received: date / Revised version: date

Abstract We formalize the coupled criterion (CC) in the framework of Finite Fracture Mechanics (FFM) to take into account the material nonlinear behavior. Once the true stress-strain curve is recorded, we estimate the Ramberg-Osgood (RO) parameters. We then exploit these values in the FFM numerical implementation, considering both an average stress requirement and the energy balance. As a case study, we consider experimental data on Brazilian disks containing a circular hole and involving two materials - PMMA and GPPS. The computational effort of the analysis increases with respect to the linear elastic case, but keeps reasonable. On the other hand, the nonlinear FFM investigation allows a significant improvement of the failure stress predictions, especially those related to smaller holes corresponding to a more pronounced nonlinear behavior detected during tests.

Keywords: Finite Fracture Mechanics; Ramberg-Osgood model; Nonlinearities, Brazilian disk tests; Circular holes

1 Introduction

Linear elastic fracture mechanics (LEFM) allows studying the propagation of an existing crack but fails to predict its nucleation. Crack initiation in brittle materials can be modeled using several methods such as, *e.g.*, cohesive zone models [1,4,5,11, 13,29,43] or phase-field models for fracture [2,31, 32]. An approach that has been specifically developed in the framework of Finite Fracture Mechanics (FFM) [15,33] so as to model crack initiation is the coupled criterion (CC) [18], which allows both the initiation loading and crack length to be determined by simultaneously fulfilling a stress condition and the energy balance. This approach has already been applied to predict crack initiation in a broad range of materials (such as *e.g.*, composites [6,7,14, 28], ceramics [20,22,30]), configurations (interfaces [25–27,40], V-notch [4,19,21]) or loading conditions [10,36]. A review of these applications was presented by Weißgraeber *et al.* [44]. The CC requires only two fracture parameters as input, namely the material strength and fracture toughness. Moreover, compared to other methods cited previously, one advantage of the CC is its numerical efficiency [11]. As a matter of fact, under the assumption of small deformations, only one calculation is needed to compute the stress criterion, and few calculations with varying crack size are needed to compute the energy balance. Besides, since the fracture parameters are only implemented during the post-processing step, no extra calculations are needed to predict crack initiation for another set of material properties. This is particularly useful when these parameters are not known and must be determined by an indirect confrontation with experimental data [8,9].

Until now, the CC has been mainly applied in a linear elastic framework and under the assumption of small deformations. There are only few applications involving nonlinearities [17,21,35,23]. Leite *et al.* [17] modeled fracture of open hole plate under tension [24] using either linear elastic or nonlinear material behavior. The expected improved agreement with respect to experimental results using the nonlinear elastic behavior was missing. Leguillon and Yosibash [21] studied crack initiation at a V-notch including a small damaged or plastic zone ahead of the notch tip, which was modeled by a decrease in the Young's modulus and varying fracture properties in this zone. The CC was applied using matched asymptotic expansions under the assumption of a small damage area near the V-notch. Two nested loops were implemented in order to both analyze the variation of the material parameters with dam-

age and compute crack initiation using the CC. The analysis was however limited to a theoretical framework, lacking a comparison with experimental data. Rosendahl *et al.* [35] applied the CC in case of adhesive connections bonded using structural silicone sealants, which undergo large deformations before failure. A stretch criterion was implemented instead of the classical stress criterion to better represent distortional bulk failure surfaces. Recently, Li *et al.* [23] proposed a numerical implementation of the CC for damaged material. The damaged field in the material was computed using continuum damage mechanics and associated regularization techniques, while the transition from continuous damage field to a discontinuous crack (using element removal strategy) was determined using the CC. The proposed numerical procedure was applied to several examples including single crack initiation and growth, as well as multicracking.

In a previous study, Torabi *et al.* [42] compared the initiation stress predicted using the CC with experimental data obtained by carrying out Brazilian disk (BD) tests on PMMA and GPPS specimens with circular holes. The application of the CC in a linear elastic framework led to a good matching except for small holes, due to some nonlinear phenomena disregarded by the model [42]. A similar conclusion was drawn by Doitrand and Leguillon [8] in case of aluminum specimens bonded with an epoxy layer, for which neglecting material nonlinearities could explain the bigger discrepancy between numerical predictions and experimental data obtained for the smallest layers.

The objective of this paper is the implementation of the CC in a nonlinear framework. The studied case is that of BD with circular holes mentioned above [42], which is described in Section 3. In Section 2, the CC in a nonlinear framework is presented. The geometry of BD and the Finite Element (FE) model are described in Section 4. In Section 5, crack initiation predictions obtained using both a linear elastic and a nonlinear material behavior are compared to experimental results taken from [42].

2 FFM Nonlinear implementation

In the framework of FFM, crack initiation under quasi-static loading conditions requires the simultaneous fulfillment of two separate conditions [18]. First, the stress state must be high enough over the whole expected crack path prior to crack nucleation. This condition, originally proposed by Leguillon [18], consists in comparing the stress normal to the crack plane σ_{nn} with the material strength σ_{c}. This condition can also be replaced by a condition involving the average stress over the crack length l, as proposed, *e.g.*, in [3,37,39]:

$$\overline{\sigma}_{\mathrm{nn}}(l) = \frac{1}{l}\int_0^l \sigma_{\mathrm{nn}}(s)ds \geq \sigma_{\mathrm{c}} \tag{1}$$

To be consistent with the previous work about failure predictions in Brazilian disk tests [42], condition 1 will be implemented, the comparison between the approaches going beyond the scope of this paper. The second condition that must be fulfilled can be obtained through a balance of the potential (δW_{p}), kinetic (δW_{k}), and crack surface formation ($G_{\mathrm{c}}l$, G_{c} being the material critical energy release rate) energies between a state before and after crack nucleation. Quasi-static initial conditions lead to a production of kinetic energy ($\delta W_{\mathrm{k}} \geq 0$) allowing the energy condition to be derived, which consists in comparing the incremental energy release rate G^{inc} with G_{c}.

$$G^{\mathrm{inc}}(l) = \frac{W_p(0) - W_p(l)}{l} \geq G_{\mathrm{c}} \tag{2}$$

It can be noted that the energy dissipated by non-linear mechanisms is not accounted for in the energy balance. As stated in introduction, the application of the CC in a linear elastic framework and under the small deformation assumption only requires few calculations to be performed. In this case, the stress is proportional to the imposed load or displacement U and the potential energy of both the damaged and the undamaged material is proportional to the square of applied load:

$$\begin{cases} \sigma_{\mathrm{nn}}(l,U) = k(l)U = \sigma_{\mathrm{c}} \\ G^{\mathrm{inc}}(l,U) = A(l)U^2 = G_{\mathrm{c}} \end{cases} \tag{3}$$

where A and k are functions depending only on the material parameters and specimen geometry. Therefore, the stress prior to crack initiation and the incremental energy release rate can be computed once for any load level U. The combination of both criteria leads to the determination of the initiation load U_{c} and crack length l_{c} [11,18] by solving:

$$\frac{k(l_{\mathrm{c}})^2}{A(l_{\mathrm{c}})} = \frac{\sigma_{\mathrm{c}}^2}{G_{\mathrm{c}}}. \tag{4}$$

If nonlinearities are accounted for, originating for instance from the material behavior (*e.g.*, non linear stress-strain curves or large deformations) or from the simulation features (*e.g.*, contact between several parts), the proportionality of the stress and the potential energy to respectively the load and the square load is no longer ensured. In this case, from a rigorous point of view, it is necessary to compute the stress and the energy conditions for several loading levels and determine the minimum loading level U_c

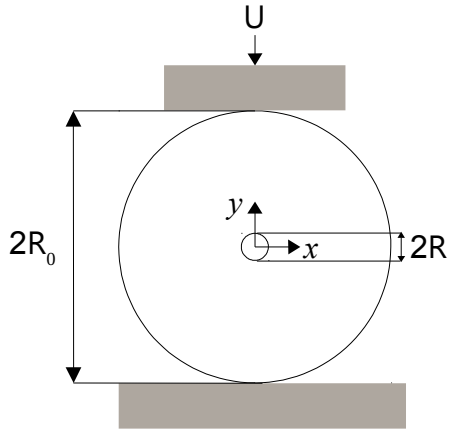

Fig. 1 Brazilian disk specimen containing a circular hole.

for which both conditions are fulfilled which can be achieved by solving the following minimization problem:

$$U_{\rm c} = \min\{U, \exists l, (\frac{G^{\rm inc}(l,U)}{G_{\rm c}} \geq 1) \wedge (\frac{\sigma_{\rm nn}(l,U)}{\sigma_{\rm c}} \geq 1)\} \tag{5}$$

The initiation crack length thus verifies :

$$\min(\frac{G^{\rm inc}(l_{\rm c},U_{\rm c})}{G_{\rm c}}, \frac{\sigma_{\rm nn}(l_{\rm c},U_{\rm c})}{\sigma_{\rm c}}) = 1 \tag{6}$$

The practical implementation of the CC solution in a nonlinear framework is discussed more in Section 4.

3 Experimental tests and data

Let us consider the Brazilian disk tests carried out in [42]. The geometry of the samples is reported in Fig. 1. Some experimental tests aiming at determining fracture initiation were performed by Torabi *et al.* [42] on t=10mm (PMMA) or t =8mm (GPPS) thick specimens with R_0=40mm and different hole sizes corresponding to R = 0.25, 0.5, 1, 2 and 4mm. For all the tested configuration, brittle fracture occurred with crack initiation from the hole edge in the loading direction. Torabi *et al.* [42] determined the failure stress as a function of the hole radius for both PMMA and GPPS specimens, highlighting the size effects of a decreasing initiation stress with an increasing radius. In the following, the experimental results used for the comparison with numerical predictions are taken from [42]. The true stress-strain curves of specimens without holes under uniaxial tensile loading are given in Fig. 2. The material behavior is slightly non linear and can be well reproduced numerically using the RO model [34].

$$\epsilon = \frac{\sigma}{E} + \alpha\frac{\sigma}{E}(\frac{\sigma}{\sigma_0})^{n-1} \tag{7}$$

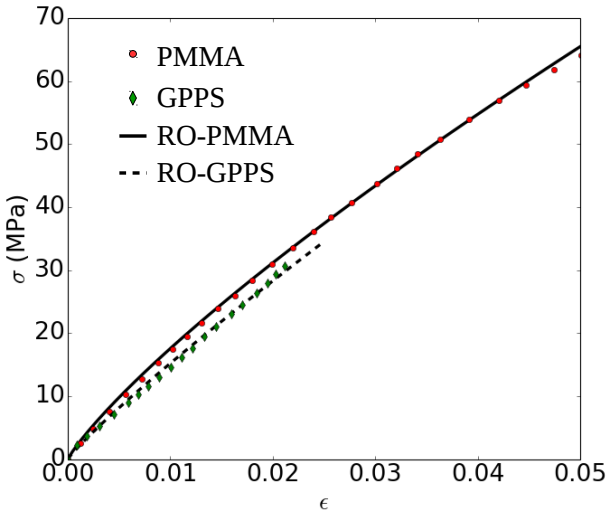

Fig. 2 Experimental (dots and diamonds) and simulated with Ramberg-Osgood (RO) model (dashed and full lines) stress-strain curves for PMMA and GPPS specimen without hole.

Table 1 Material properties for PMMA and GPPS.

	PMMA	GPPS
E (MPa)	2960	3100
ν	0.38	0.34
α	2	1.9
σ_0 (MPa)	68	30
n	1.4	1.2
$\sigma_{\rm c}$ (MPa)	78	40
$G_{\rm c}$ (MPa.mm)	0.88	0.23
L_{mat} (mm)	0.428	0.446

The corresponding parameters are given in Table 1 together with the strength and fracture toughness of both materials taken from [42]. The Ramberg-Osgood parameters were determined by means of FE calculations on specimens without hole under uniaxial tensile loading so as to fit the experimental stress-strain curves.

4 Finite element analysis

A 2D plane strain FE model of Brazilian disk test is set-up using Abaqus$^{\rm TM}$. As demonstrated in [12], compared to the 3D case, it may be representative of the specimen middle plane. Due to the specimen and test symmetry, only one quarter of the specimen can be modeled. The platen is modeled as infinitely rigid and a displacement of the platen in (Oy) direction is imposed as boundary condition. Contact between the platen and the specimen is taken into account using a normal hard contact and no tangential friction, making the calculations nonlinear. Therefore, even if a linear elastic material behavior is used, the

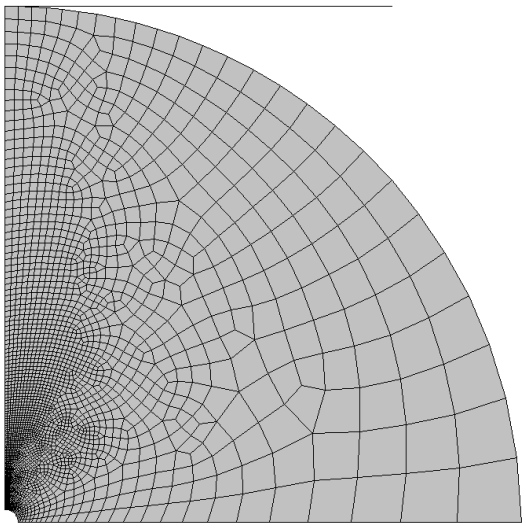

Fig. 3 Mesh of one quarter of the Brazilian disk specimen.

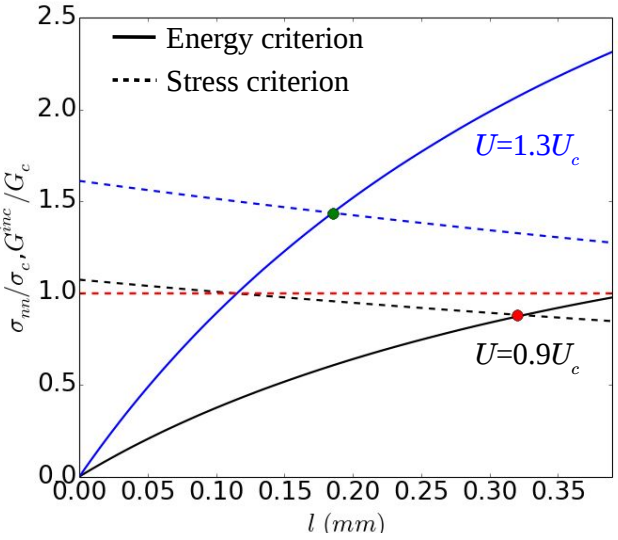

Fig. 4 Incremental energy release rate to fracture toughness and stress to strength ratios variation as a function of the crack length l for imposed loading $U = 0.9U_c$ and $U = 1.3U_c$

nonlinear solution of the CC as presented in Section 2 must be adopted. The uniaxial compression in (Oy) direction leads to crack initiation in the same direction due to the specimen lateral expansion. Experimentally, it was not possible to check whether symmetric or asymmetric crack initiation occurred [42]. However, the discrepancy between symmetric or asymmetric crack initiation predicted by the CC in such configurations is generally small [38,42]. Therefore, symmetric crack initiation is assumed so as to be consistent with [42]. The material parameters of either linear elastic or nonlinear elastic (Ramberg-Osgood model) material behavior are implemented (Table 1).Solving the CC requires a mesh that is fine enough so as to capture the initiation crack length. It can be shown that this length is a fraction of the material characteristic length $L_{mat} = \frac{EG_c}{\sigma_c^2}$ [30]. Fig. 3 shows an example of Brazilian disk specimen mesh consisting of four-nodes linear elements. The minimum mesh size is set to $5{\times}10^{-3}$mm and a progressive unrefinement of the mesh along the crack path is performed, as explained in [11]. The FE model consists in about 5000 nodes and the typical duration for one calculation is 30s.

Applying the CC to the case of Brazilian disk specimens requires Eq. (5) to be solved. An approach similar to that proposed in [17] is adopted herein. In practice, a discretization of the imposed displacement $\{U_k\}_{k=1..n}$ can be chosen so as to solve Eq. (5). For each loading level U_k, one calculation is required so as to compute the stress condition of the CC (Eq. (1)) whereas several calculations with varying crack length are needed to compute the energy condition (Eq. (2)). For a given loading level, around 100 calculations with varying crack length are performed to compute the potential energy difference due to crack initiation and hence the incremental energy release rate. This is done by progressive releasing of the symmetry condition of the nodes lying on the crack path. At each loading level, it is checked whether the CC is fulfilled or not. Then, the initiation loading level is determined using Eq. (5) by interpolation of the computed values. Fig 4 shows the variation of (i) stress to strength and (ii) incremental energy release rate to fracture toughness ratios for two imposed displacement levels for which the CC is fulfilled or not. It can be seen that in both cases, a solution to Eq. (4) can be found, which allows determining l_c. However, a sufficiently high imposed loading must be prescribed so that a solution to Eq. (5) can be found. Fig 5 shows the incremental energy release rate to fracture toughness ratios evaluated for l_c as a function of the imposed displacement. In the present case, 5 imposed displacement values were used to compute the CC and determine at least one imposed displacement for which the CC is fulfilled. Then, the initiation displacement and crack length are determined by interpolating the values computed on the basis of the discretized imposed displacement. It can be noted that despite the nonlinear CC solution requires more calculations than the usual linear application, they can be executed in parallel. In the present work, 5 calculations were performed in parallel so that the overall analysis for a given hole size specimen finally take around 30 minutes, which is still reasonable compared to the overall analysis time of the classical approach [11]. Note that, in addition, once the calculations are performed, the fracture properties of the material can be easily varied

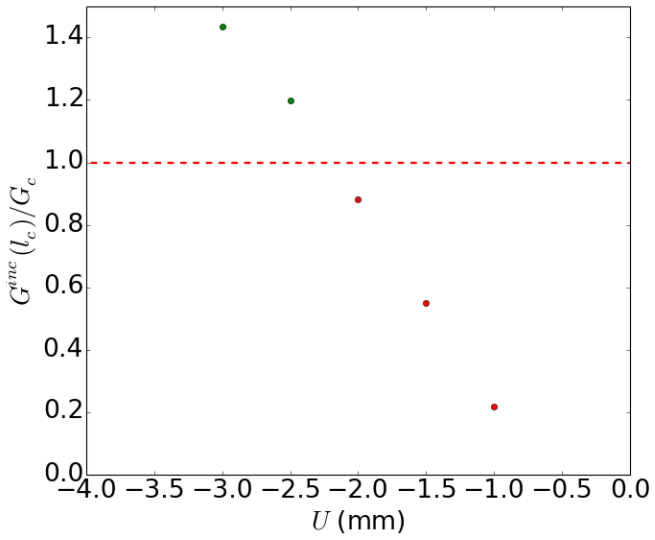

Fig. 5 Incremental energy release rate to fracture toughness ratio evaluated for $l = l_c$ as a function of the imposed loading U.

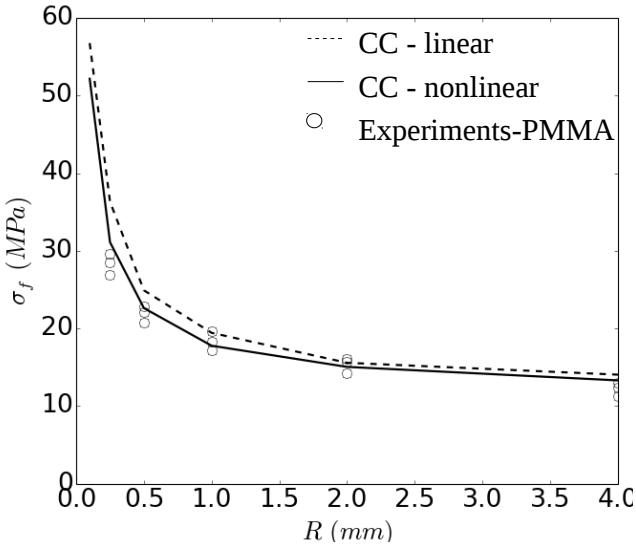

Fig. 6 Failure stress σ_f as a function of hole radius R for PMMA samples.

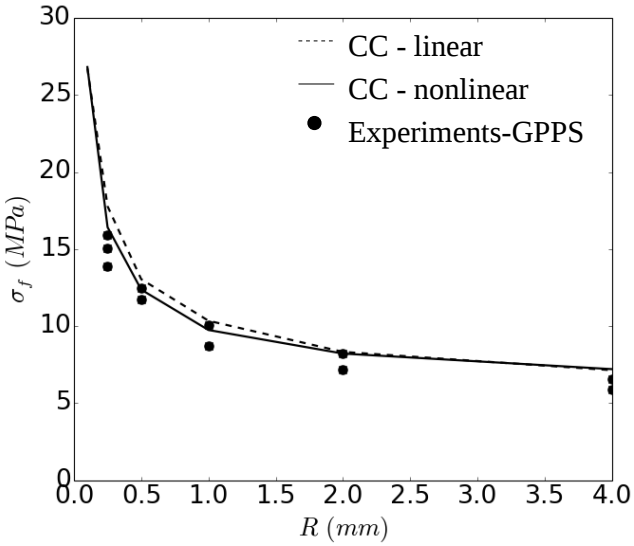

Fig. 7 Failure stress σ_f as a function of the hole radius R for GPPS samples.

without any extra calculations since they are only implemented during the post-processing step, which is a main advantage of the CC.

5 Results and discussions

The solution of the CC in nonlinear framework is now applied to the case of PMMA or GPPS Brazilian disk specimens including a central hole. For each case, the critical imposed displacement is computed according to the procedure presented in Section 2. The associated reaction force F_c is then estimated so as to obtain the equivalent failure stress σ_f given by the following expression [16,42]:

$$\sigma_f = \frac{F_c}{\pi R_0 t} \tag{8}$$

Figs. 6 and 7 show the failure stress predicted by the CC using either a linear elastic or a nonlinear material behavior. It can be seen that the hole size effect is very well captured by the CC whatever the material behavior since similar trends as experimentally are obtained numerically. Implementing a linear instead of a nonlinear material behavior results in overestimating of the failure stress. The discrepancy between both cases remains lower than 10% for PMMA and 15% for GPPS. Taking into account the material nonlinear behavior allows reducing the discrepancy with respect to the mean value of experimental data (Tables 2 and 3), especially for the smallest holes. For instance, the difference between predictions and mean experimental failure stress is reduced from 27.9% to 9.6% for PMMA and from 18.5% to 9.4% for GPPS in the case of the $R = 0.25$mm hole radius.

6 Conclusions

The CC has been implemented in a nonlinear framework for failure stress prediction in Brazilian disk specimens. Nonlinearities originate from both the contact between the platen and the specimen and the material stress-strain curves. Concerning the FE implementation, taking nonlinearities into account requires more calculations to be performed since there is no longer any proportionality between the stress and the load, and between the potential energy and the square load. Therefore, the dependency of stress

Table 2 Deviation between failure stress predictions with the CC using either a linear elastic or a nonlinear material behavior and mean experimental failure stresses for PMMA specimens.

Hole radius	$\frac{\Delta\sigma_f}{\sigma_f}$ (linear) (%)	$\frac{\Delta\sigma_f}{\sigma_f}$ (nonlinear) (%)
0.25	27.9	9.6
0.5	13.2	2.7
1	5.	3.6
2	0.01	2.9
4	14.7	3.97

Table 3 Deviation between failure stress prediction with the CC using either a linear elastic or a nonlinear material behavior and mean experimental failure stresses for GPPS specimens.

Hole radius	$\frac{\Delta\sigma_f}{\sigma_f}$ (linear) (%)	$\frac{\Delta\sigma_f}{\sigma_f}$ (nonlinear) (%)
0.25	18.5	9.4
0.5	8.8	3.2
1	11.2	4.7
2	7.7	6.3
4	13.7	14.8

and energy to the applied load has to be computed for several load levels, looking for the minimum load for which both criteria are fulfilled.

It is important to note that the fracture parameters G_c and σ_c are only implemented during the post-processing step. Therefore once the calculations are performed for a given configuration, it is easy to vary these fracture parameters without any additional computational costs, contrary to other fracture approaches such as cohesive zone modeling or phase field models for fracture.

Applying the CC to crack initiation prediction in Brazilian disk specimens with circular holes using linear elastic material behavior results in a reasonable matching except for small holes for which crack initiation occurs at higher loading level and thus with more pronounced nonlinearities. Taking into account the nonlinear material behavior allows to remove this drawback, improving significantly the theoretical FFM predictions.

References

1. Barenblatt, G.I. ,1959. The formation of equilibrium cracks during brittle fracture: general ideas and hypotheses. Axially-symmetric Cracks PMM 23, 622-636.
2. Bourdin, B., Francfort, G.A., Marigo, J.J., 2000. Numerical experiments in revisited brittle fracture. J. Mech. Phy. Sol. 48, 797-826.
3. Cornetti, P., Pugno, N., Carpinteri, A., Taylor D. Finite fracture mechanics: a coupled stress and energy failure criterion, Engng. Fract. Mech. 73(14), 2021-2033.
4. Cornetti, P., Sapora, A., Carpinteri, A., 2016. Short cracks and V-notches: Finite Fracture Mechanics vs. Cohesive Crack Model. Engng. Fract. Mech. 168, 2-12.
5. Cornetti, P., Munũnoz-Reja, M., Sapora, A., Carpinteri, A, 2019. Finite Fracture Mechanics and cohesive crack model: weight functions vs. cohesive laws. Int. J. Sol. Struct. 156-157, 126-136.
6. Doitrand, A., Fagiano, C., Carrère, N., Chiaruttini, V., Hirsekorn, M., 2017. Damage onset modeling in woven composites based on a coupled stress and energy criterion. Engng. Fract. Mech. 169, 189-200.
7. Doitrand, A., Fagiano, C., Hild F., Chiaruttini, V., Mavel A., Hirsekorn, M., 2017. Mesoscale analysis of damage growth in woven composites Compos Part A. 96, 77-88.
8. Doitrand, A., Leguillon, D, 2018. 3D application of the coupled criterion to crack initiation prediction in epoxy/aluminum specimens under four point bending. Int. J. Sol. Struct 143, 175-182.
9. Doitrand, A., Leguillon, D, 2018. Comparison between 2D and 3D applications of the coupled criterion to crack initiation prediction in scarf adhesive joints. Int. J. Adh. Adh. 85, 69-76.
10. Doitrand, A., Leguillon, D. Numerical modeling of the nucleation of facets ahead of a primary crack under mode I+III loading. Int. J. Fract. 213, 37-50.
11. Doitrand, A., Estevez, R., Leguillon, D., 2019. Comparison between cohesive zone and coupled criterion modeling of crack initiation in rhombus hole specimens under quasi-static compression. Theor. Appl. Fract. Mech. 99, 51-59.
12. Doitrand, A., Estevez, R., Leguillon, D., 2019. Experimental characterization and numerical modeling of crack initiation in rhombus hole PMMA specimens under compression. Eur. J. Mech. A/Sol. 76, 290-299.
13. Dugdale, D.S., 1960. Yielding of steel sheets containing slits. J. Mech. Phys. Sol 8,100-104.
14. García, I.G., Carter, B.J., Ingraffea, A.R., Mantič V., 2016. A numerical study of transverse cracking in cross-ply laminates by 3D finite fracture mechanics. Compos. Part B 95, 475-487.
15. Hashin, Z.,1996. Finite thermoelastic fracture criterion with application to laminate cracking analysis. J. Mech. Phys. Solids 44(7), 1129-1145.
16. Hobbs DW., 1965. An assessment of a technique for determining the tensile strength of rock. Br. J. Appl. Phys. 16, 259-68.
17. Leite, A., Mantič, V., París, F. Application of finite fracture mechanics to composites: crack onset in a

stretched open hole polymer plate with nonlinear behaviour. ECCM16, Seville, Spain, 22-26 June 2014.
18. Leguillon, D., 2002. Strength or toughness? A criterion for crack onset at a notch. Eur. J. Mech. - A/Solids 21 (1), 61-72.
19. Leguillon, D. , Quesada, D. , Putot, C. , Martin, E. , 2007. Size effects for crack initiation at blunt notches or cavities. Engng. Fract. Mech. 74, 2420-2436 .
20. Leguillon, D., Martin, E., Seveček, O., Bermejo, R. (2015). Application of the coupled stress-energy criterion to predict the fracture behaviour of layered ceramics designed with internal compressive stresses. Eur. J. Mech. A/Solids, 54, 94-104.
21. Leguillon, D., Yosibash, Z., 2017. Failure initiation at V-notch tips in quasi-brittle materials. Int. J. Solids Structures, 122-123, 1-13.
22. Leguillon, D., Martin, E., Seveček, O., Bermejo R, 2018. What is the tensile strength of a ceramic to be used in numerical models for predicting crack initiation? Int. J. Fract. 212(1), 89-103.
23. Li, J., Leguillon, D., Martin, E., Zhang, X.B., 2019. Numerical implementation of the coupled criterion for damaged materials. Int. J. Sol. A/Struct. 165, 93-103.
24. Li, J., Zhang, X, 2006. A criterion study for nonsingular stress concentrations in brittle or quasi-brittle materials. Engng. Fract. Mech. 73, 505-23.
25. Mantič, V., 2009. Interface crack onset at a circular cylindrical inclusion under a remote transverse tension. Application of a coupled stress and energy criterion. Int. J. Sol. Struct. 46, 1287-1304.
26. Mantič, V., García, I.G., 2012. Crack onset and growth at the fibre-matrix interface under a remote biaxial transverse load. Application of a coupled stress and energy criterion. Int. J. Solids Structures 49, 2273-2290.
27. Martin, E., Poitou, B., Leguillon, D., Gatt, J.M., 2008. Competition between deflection and penetration at an interface in the vicinity of a main crack. Int. J. Fract. 151(2), 247-268.
28. Martin, E., Leguillon, D., Carrère, N., 2012. A coupled strength and toughness criterion for the prediction of the open hole tensile strength of a composite plate. Int. J. Solids and Structures 49 (26), 3915-3922.
29. Martin, E., Vandellos, T., Leguillon, D., Carrère, N., 2016. Initiation of edge debonding: coupled criterion versus cohesive zone model. International Journal of Fracture. 199, 157-168.
30. Martin, E., Leguillon, D., Seveček, O., Bermejo, R., 2018. Understanding the tensile strength of ceramics in the presence of small critical flaws. Engng. Fract. Mech. 201, 167-175.
31. Miehe, C., Welschinger, F., Hofacker, M., 2010. Thermodynamically consistent phase-field models of fracture: Variational principles and multi-field FE implementations. Int. J. Num. Meth. Engng. 83, 1273-1311.
32. Molnar, G., Gravouil, A., 2017. 2D and 3D Abaqus implementation of a robust staggered phase field solution for modeling brittle fracture. Finite Elem. Ana. Des. 130, 27-28.
33. Nairn, J.A., 2000. Exact and variational theorems for fracture mechanics of composites with residual stresses, traction-loaded cracks and imperfect interfaces. Int J Fract 105:243-271.
34. Ramberg, W., Osgood, W.R., 1943. Description of stress-strain curves by three parameters. Technical Note No. 902, National Advisory Committee For Aeronautics, Washington DC
35. Rosendahl, P.L., Drass, M., Schneider, J., Becker, W. (2018). Crack nucleation in hyperelastic adhesive bonds. Ce/Papers 2(5-6), pp. 409-425
36. Sapora A., Cornetti P., 2014. Carpinteri V-notched elements under mode II loading conditions. Struct. Engng. Mech. 49, 499-508.
37. Sapora, A., Cornetti, P., Carpinteri, A., Firrao, D, 2015. An improved Finite Fracture Mechanics approach to blunt V-notch brittle fracture mechanics: Experimental verification on ceramic, metallic,and plastic materials. Theor. Appl. Fract. Mech. 78, 20-24.
38. Sapora, A., Cornetti, P., 2017. Symmetric vs. asymmetric crack initiation from a circular hole. In: Proceedings of the International Symposium on Notch Fracture, Santander, Spain, March 29-31; 2017.
39. Sapora, A., Cornetti, P., 2018. Crack onset and propagation stability from a circular hole under biaxial loading. Int. J. Fract. 214, 97-104.
40. Stein, N., Weigraeber, P., Becker, W., 2015. A model for brittle failure in adhesive lap joints of arbitrary joint configuration. Compos Struct 133, 707-718.
41. Talmon l'Armée, A., Hell, S., Rosendahl, P.L., Felger, J., 2017. Nonlinear crack opening integral : Mode mixity for finite cracks. Engng. Fract. Mech. 186, 283-299.
42. Torabi, AR., Etesam, S., Sapora, A., Cornetti, P, 2017. Size effects on brittle fracture of Brazilian disk samples containing a circular hole. Engng. Fract. Mech. 186, 496-503.
43. Tvergaard, V., Hutchinson, J.W., 1992. The relation between crack growth resistance and fracture process parameters in elastic-plastic solids. J. Mech. Phys. Sol. 40,1377-1397.
44. Weißgraeber, P., Leguillon, D., Becker, W., 2016. A review of Finite Fracture Mechanics: crack initiation at singular and non-singular stress raisers. Archive Appl. Mech. 86 (1-2), 375-401.